Available online at www.sciencedirect.com
ScienceDirect
Journal of Sound and Vibration 311 (2008) 280–296
JOURNAL OF SOUND AND VIBRATION
www.elsevier.com/locate/jsvi

Effect of non-uniform perforation in the long concentric resonator on transmission loss and back pressure

Seong-Hyun Lee[1], Jeong-Guon Ih*

Center for Noise and Vibration Control, Department of Mechanical Engineering, Korea Advanced Institute of Science and Technology (KAIST), Taejon 305-701, Korea

Received 2 August 2007; received in revised form 2 August 2007; accepted 10 September 2007
Available online 22 October 2007

Abstract

It is known that the acoustical and, possibly, mechanical performance of the perforated resonator can be controlled by the porosity and distribution of holes. To analyze the effect of the porosity distribution pattern on resonator performance, in particular under the design condition of restricted volume, five typical perforation patterns of an acoustically long concentric resonator were investigated experimentally and numerically. Transmission loss and back pressure were used to represent the acoustic and mechanical performance indices, respectively. Prediction of transmission loss was made by segmental decoupling analysis with an empirical impedance model of orifices. Prediction of back pressure was done by computational fluid dynamics analysis. The overall trend of the calculated results matched well with the measured results. In terms of acoustic performance, it is noted that a specific frequency range was mostly influenced by the change of axial porosity pattern. For mechanical performance, a gradual change in porosity played a dominant role in stabilizing the flow field and static pressure distribution. It is concluded that an axial perforation pattern with a gradual change in porosity yields the best performance by forming a flow field with minimized loss and an acoustic field dominated by a quarter-wavelength resonance of equivalent extended pipes. In particular, the most preferred perforation pattern in terms of transmission loss and back pressure was the one with gradually increasing porosity from the upstream part and gradually decreasing porosity from the middle part as far as the downstream end.

1. Introduction

Passive silencing devices are extensively used in intake and exhaust systems of various fluid machines for attenuating combustion noise or fluid-borne noise. The principal design factors of silencers, including transmission loss (TL), back pressure, size, cost and weight, need to be adjusted to satisfy a preset design goal [1]. The two most important design targets for a silencer are to obtain noise reduction greater than the required minimum value and back pressure lower than the maximum permissible value, which are often contradictory. For example, the noise attenuation principle of reactive silencers is based on the mechanism of

*Corresponding author. Tel.: +82 42 869 3035; fax: +82 42 869 8220.
E-mail address: J.G.Ih@kaist.ac.kr (J.-G. Ih).
[1]Current address: Institute of Construction Technology, Samsung Engineering & Construction, 270-1, Seohyun-Dong, Bundang-Gu, Sungnam-Si, Gyonggi-Do 463-824, Korea.

0022-460X/$ - see front matter © 2007 Elsevier Ltd. All rights reserved.
doi:10.1016/j.jsv.2007.09.005

impedance mismatch, which causes the incident sound wave to be reflected toward the source. Such an impedance mismatch usually entails a pressure drop, leading to an additional load on the source output.

In practical use, perforated pipes are widely adopted inside the jacket of silencers. The simplest structure using a perforated inner pipe is the concentric resonator. In this case, the perforated inner tube is sometimes called the 'perforated bridge'. This perforated inner pipe has various design implications, depending on the service conditions and design target. By introducing a fully or partially perforated inner tube in a simple expansion chamber, with porosity higher than approximately 16–20%, the tube acts as a flow stream guide to prevent the flow separation and excessive turbulence at sharp discontinuities in the flow path, thus reducing flow-generated noise and pressure drops. Flow-generated noise includes noise radiated from the vortices formed at the sharp edge of the inlet, turbulence and shear flow ('whistling'), flow impinging at the endplate of the outlet side, and interaction between the impulsive acoustic loading at the outlet and the resonance of the connecting pipe (e.g., tail pipe 'singing'). For a fully perforated resonator, the acoustic performance is nearly the same as that of a simple expansion chamber of the same jacket size. For a partially perforated resonator with high porosity, the acoustic performance is nearly the same as that of a simple expansion chamber with an extended inlet and/or outlet. In addition, a perforated bridge can stiffen the whole structure of a simple expansion chamber by connecting the inlet and outlet. This reduces excessive stress at the structural joints in both termination areas, and thus lengthens the fatigue life of the silencer structure. When the porosity of the inner tube is low, i.e., far less than about 16%, a perforated inner tube can be used to reduce some specific bands or to attain broadband sound attenuation by controlling the porosity. An extended inlet and/or outlet can be combined with this low porosity to achieve a large attenuation in the same bands. Sometimes, a perforated pipe can be used to suppress high-order modes, thus extending the applicable frequency range while suppressing adverse effects due to flow.

In many practical cases, orifices in the concentric resonator are uniformly distributed on the inner pipes. Depending on the perforation distribution pattern, the mechanical and acoustic performance are uniquely determined for a given service condition [2]. Shenoda [3] suggested two types of perforation distribution patterns with good performance by testing silencers mounted on the exhaust system of a diesel engine. A weighted insertion loss and back pressure were used to represent the acoustic and mechanical performances. It was suggested that optimized performance could be attained using a resonator with a perforated tube of gradually changing porosity: minimum porosity at both ends of the inner pipe and maximum porosity at the middle of the inner tube. However, except for a simple comment on impedance matching at the ends of the inner pipe, no detailed reason for the good performance of a specific hole distribution pattern was given. There was no comparison with other distribution patterns, such as uniform distribution, which are typically used in commercial silencers. Kim and Yoon [4] experimentally investigated the acoustic characteristics of perforated pipes open to the free field. The TL of perforated pipes without an enclosing cavity was analyzed by varying the average porosity and the distance between the orifices. However, the results could not be directly applied to the design of actual resonators because the acoustic performance of such a perforated tube combined with an outer jacket to form a resonator was not investigated and the mechanical performance was, of course, not evaluated either.

In this work, the acoustic and mechanical characteristics of various resonators with different perforation patterns of the same average porosity were investigated by experiments and simulations. For this purpose, TL and back pressure of five concentric resonators having different perforation patterns on the inner pipe are considered. Experimentally observed trend in TL needs to be investigated theoretically to confirm the spectral behavior. To this end, the decoupling analysis method [5–8] was used with an empirical impedance model of the orifices [9] and the sectional transfer matrix method was applied to deal with the varying porosity in the pipe. The back pressure and flow field were calculated numerically by CFD analysis.

2. Effect of non-uniform porosity

Because non-uniform perforation is not physically possible for typical acoustically short chambers [10,11], this study was confined to acoustically long concentric resonators. Here, the acoustically long chamber has a length/diameter ratio greater than approximately 0.43 [12]. The concentric resonator used is shown in Fig. 1 and the perforation pattern of the inner pipe was varied. The diameters of the inner and outer cavities were 32

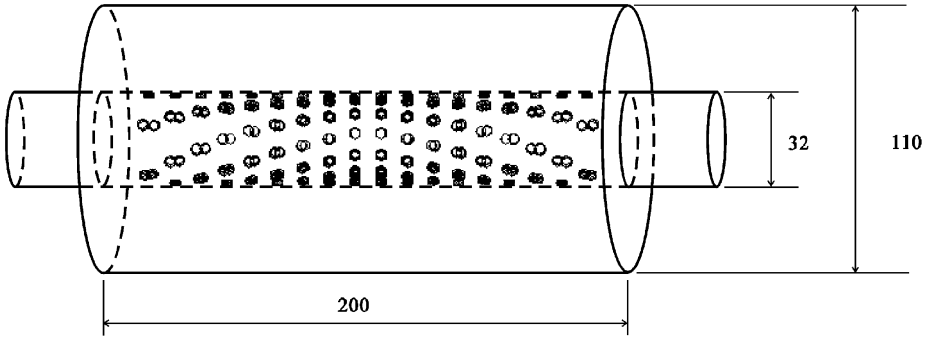

Fig. 1. Geometric shape and size of an acoustically long concentric resonator (dimensions in mm).

Table 1
Distribution patterns of perforated element used as the inner tube in a concentric resonator

Pattern no.	Porosity (%)
1	10.3 (uniform)
2	5.7–14.9 (monotonic increase)
3	14.9–5.7 (monotonic decrease)
4	5.7–14.9–5.7 (increase–decrease)
5	14.9–5.7–14.9 (decrease–increase)

and 110 mm, respectively, and the length of the resonator was 200 mm. The test silencer was made to be axisymmetric that the cut-off frequency of the first radial mode became the high-frequency limit of plane wave. The (0,1) mode would cut on at 3.8 kHz for free acoustic propagation across a tube of 110 mm in diameter. The diameter and thickness of the orifices on the perforated inner tube were 4 and 2 mm, respectively. Distribution patterns for simulation and measurement are shown in Table 1 and Fig. 2, in which porosity in the axial direction is the main parameter. Pattern 1 is the usual perforation pattern, which is uniformly perforated with a porosity of 10.3%. The average porosity of patterns 2–5 is the same as pattern 1, i.e., 10.3%. In the inner tube of pattern 2, the perforation ratio increases monotonically from 5.7% to 14.9% with increasing axial distance from the inlet region. The perforation distribution of pattern 3 is opposite to pattern 2, i.e., monotonically decreasing gradually. It should be noted that 10.3% porosity is neither high nor low in terms of resonator characteristics, so the acoustic performance preserves the basic spectral characteristics of a fully perforated resonator, but the local hole impedance plays some role. Pattern 4 has the smoothest change in wall impedance along axial distance of all the patterns: the porosity gradually increases first from 5.7% until the middle part (14.9%), then gradually decreases to the initial porosity (5.7%) near the outlet region. Pattern 5 has two sudden changes in porosity at the inlet and outlet parts of the inner tube: the porosity pattern is exactly opposite of pattern 4.

2.1. Acoustic performance

2.1.1. Measurement of TL

TL was measured using the experimental setup illustrated in Fig. 3. Air flow with a Mach number range of 0–0.17 was supplied by a compressor through a regulating section. The midstream flow velocity was measured using a Pitot tube and micro-manometer (Furness Controls, FC012). The air temperature in the test duct was 26 °C during experiments. A compression driver (50 W of output power; 180 Hz low cut-off frequency) was installed 1 m upstream from the test muffler. A swept sine signal was used for excitation to have a high signal/noise ratio. To minimize the negative effects of reflective waves from the duct end, an anechoic termination was installed at the termination, of which the reflection coefficient was less than 0.1 within the valid frequency range. The TL of a test muffler was obtained according to the following equation using the measured

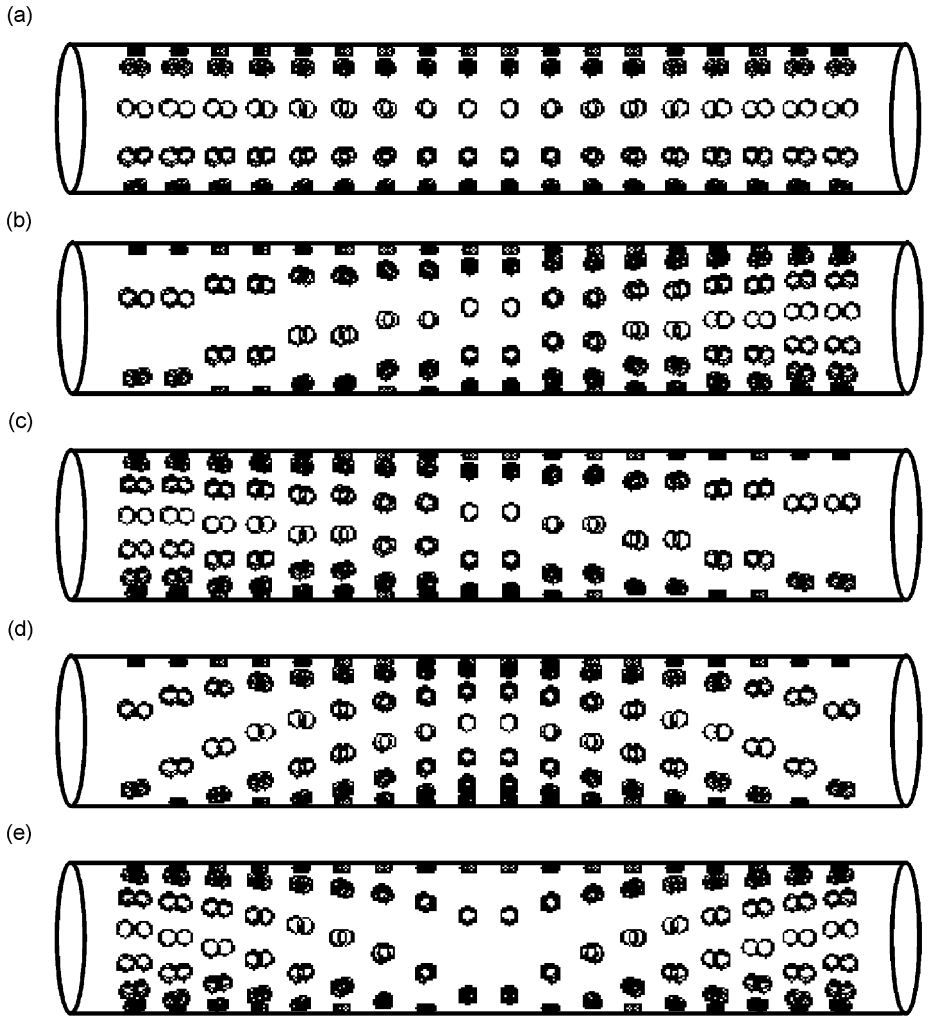

Fig. 2. Distribution patterns of perforated elements. (a) Pattern 1; (b) pattern 2; (c) pattern 3; (d) pattern 4; (e) pattern 5.

parameters [13]:

$$\mathrm{TL} = 20\log_{10}\left|\frac{1+R_d}{1+R_u}\right| - 20\log_{10}|H_{ud}|. \tag{1}$$

Here, R_d and R_u are the downstream and upstream reflection coefficients, respectively, and H_{ud} is the transfer function between the two microphones located upstream and downstream of the muffler. The three values were all measured by flush-mounted quarter-inch microphones (B&K 4135). Generation of the source signal and analysis of the measured signal were carried out by a dynamic signal analyzer (HP35670A). To obtain the reflection coefficients having small errors, a microphone array comprised of three microphones in tandem was used [14]. The spacing of adjacent microphones was 35 mm, which limited the valid frequency range to 490 Hz–4.41 kHz. The number of average in obtaining the frequency response functions was 300. To suppress errors due to turbulence noise of the air flow, a correlation technique [15] was employed. The sound pressure measured at a microphone located 0.8 m away from the first microphone of the upstream microphone array was used as the reference signal in applying the correlation technique. The reference microphone was mounted using the relation

$$ks > 2\pi M, \tag{2}$$

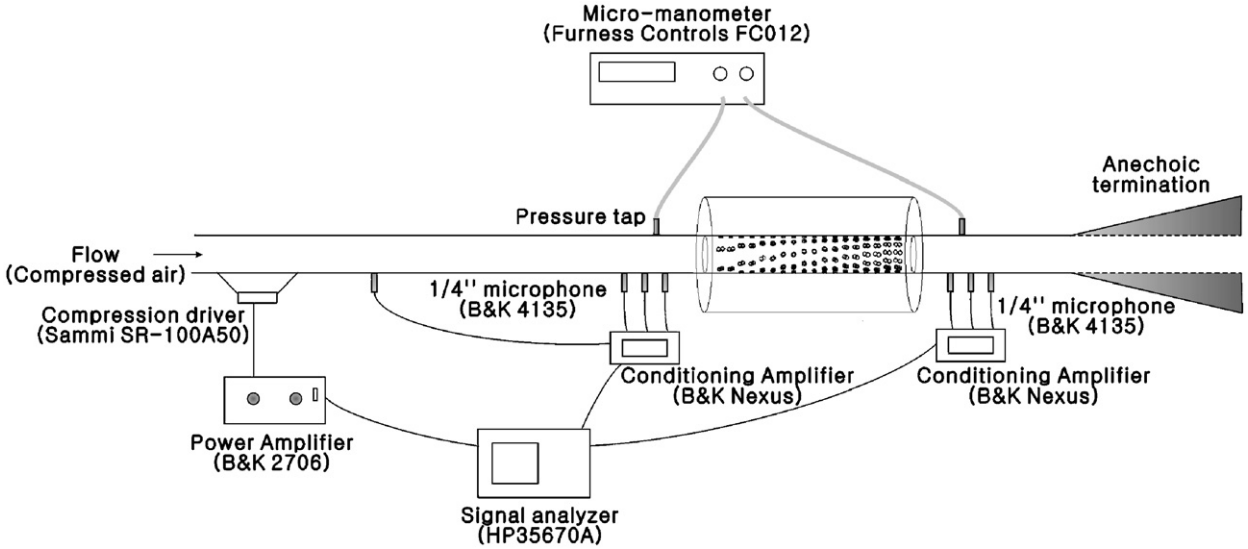

Fig. 3. Experimental setup for measuring the transmission loss and back pressure of a resonator.

where k is the wavenumber, M the mean-flow Mach number inside the duct, and s the distance between the reference microphone and the nearest microphone of the upstream array sensors.

Fig. 4 shows the measured TL values for perforated resonators varying the distribution pattern. Comparing the five patterns that differ in porosity distribution, one can observe that there exists a definite difference in the third lobe, which ranges from approximately 1.75–3 kHz. When the Mach number is in the range of 0–0.085, TL curves of all patterns except pattern 1 show an identical dip near 2.6 kHz. The same dip in the TL curve can be observed for $M = 0.17$ case. A comparison of patterns 1, 2, and 3 shows that they have nearly the same TL values in the absence of flow, but, for $M = 0.085$, the TL of pattern 3 is slightly greater than that of pattern 2 below 2.6 kHz, and vice versa above 2.6 kHz. However, trends in the case of $M = 0.17$ are contrary to those for $M = 0.085$ case. The overall shape of TL curves for patterns 1, 2, and 3 is similar. Comparing patterns 1, 4, and 5, pattern 5 has minimum values at all frequencies, except around 3 kHz. For $M = 0$ and $M = 0.085$, pattern 4 has the largest TL curve, except in the range 2.5–2.8 kHz. In the case of $M = 0.17$, the TL curve of pattern 1 is largest in the range 2.7–3 kHz. Considering the whole trend of TL curves, one can find that pattern 4 has the largest TL curve, patterns 1, 2, and 3 have intermediate TL values, and pattern 5 has the smallest TL curve. In summary, this means that the acoustic performance of pattern 4, with a perforation pattern of gradual increasing–decreasing porosity, is the best, and that of pattern 5, with a perforation pattern of gradual decreasing–increasing porosity, is the worst.

2.1.2. Prediction of TL

To confirm the foregoing spectral characteristics of TL, a theoretical model for the prediction of TL of concentric resonators was needed. A calculation model could yield clear data that are free from data jitter due to measurement errors. Because the porosity changes in the axial direction of the inner tube, the model should take account of this fact, and thus a segmental approach was used for this purpose. As can be observed in Fig. 5, a concentric resonator was divided into 20 sections, including 18 perforated sections. From the system of equations of mass continuity, momentum, and energy in the inner tube (main pipe) and the outer (or backing) cavity, two coupled second-order ordinary differential equations were obtained for each section. The transfer matrix of each section was calculated by decoupling these coupled second-order equations using the orifice impedance [5–8]. An empirical impedance model [9] of perforated elements under grazing flow conditions was used for decoupling analysis, assuming that there is only a small amount of cross-flow in actual situations. The overall TL of a resonator can be predicted by combining the transfer matrix obtained for every section. The segmental calculation method in this paper is different from the segmental approach used by

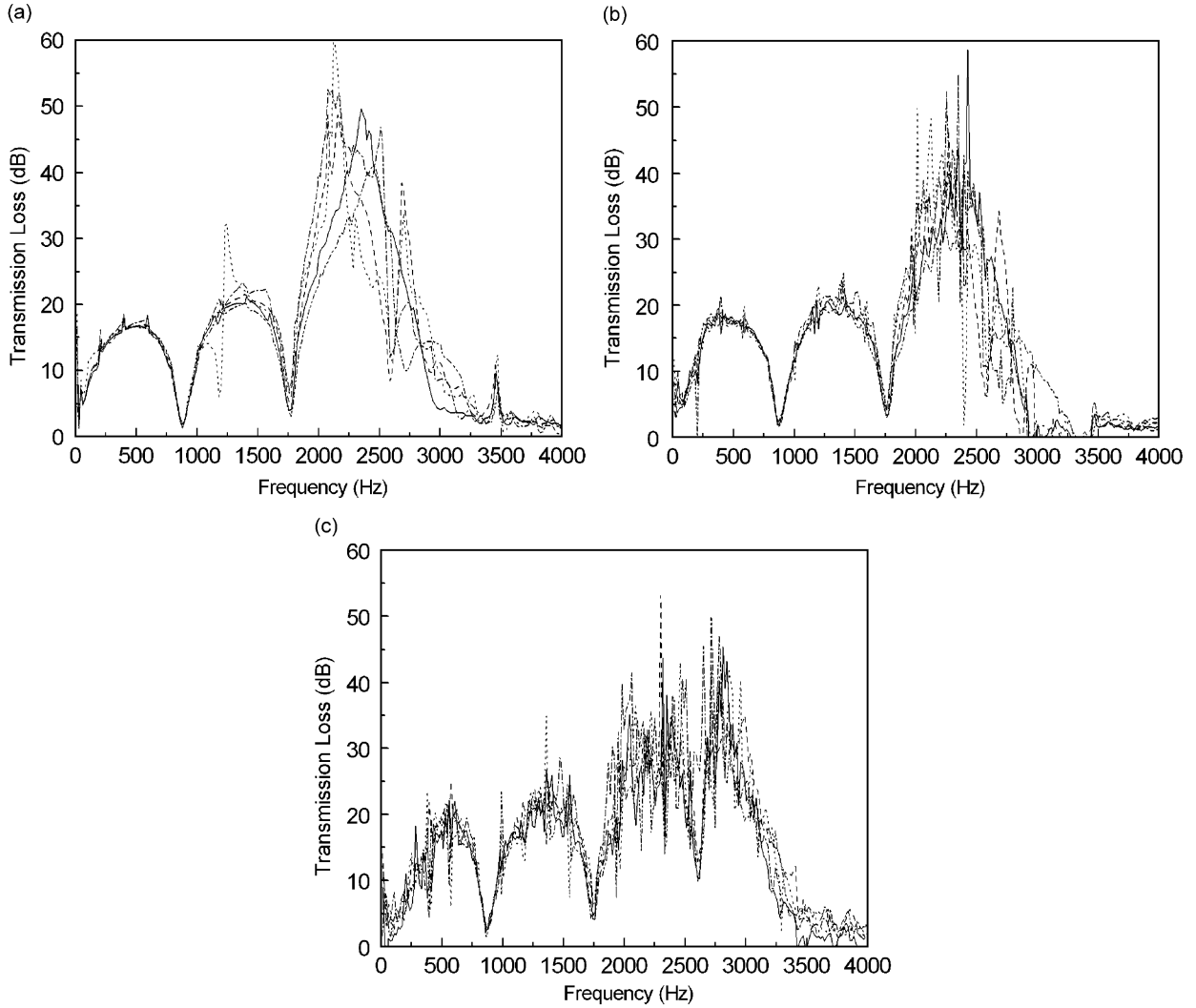

Fig. 4. Measured transmission loss for varying distribution patterns: ——, pattern 1; — —, pattern 2; - - - -, pattern 3; — - —, pattern 4; - - - -, pattern 5. (a) $M = 0.0$; (b) $M = 0.085$; (c) $M = 0.17$.

Sullivan and Crocker [10]. The latter method uses an iteration technique and the convergence of the output should be assured. It should be noted that due to the variation of porosity in the axial direction, the direction and magnitude of cross-flow velocity through perforated elements are different for every axial position. However, in the theoretical approach in this study, it was assumed that the acoustic impedance of perforates is not influenced by the cross-flow, for which the velocity is assumed to be the same and very small at all positions along the inner tube.

Predicted TL curves are presented in Fig. 6. The TL curves for patterns 2 and 3 are the same without the flow, but, on increasing the Mach number, the TL of pattern 3 is greater than for pattern 2, especially below 2.6 kHz in the third lobe. On the other hand, pattern 2 has a greater TL than pattern 3, in particular above 2.6 kHz in a third lobe, in the case of $M = 0.085$, and vice versa in the case of $M = 0.17$. Pattern 4 has the greatest and most preferable TL of all, in particular in the third and fourth lobes, and pattern 5 has an undesirable TL, regardless of flow conditions, at all frequencies of interest. It can be said that the predicted values show very similar trends to the measured values of the previous section.

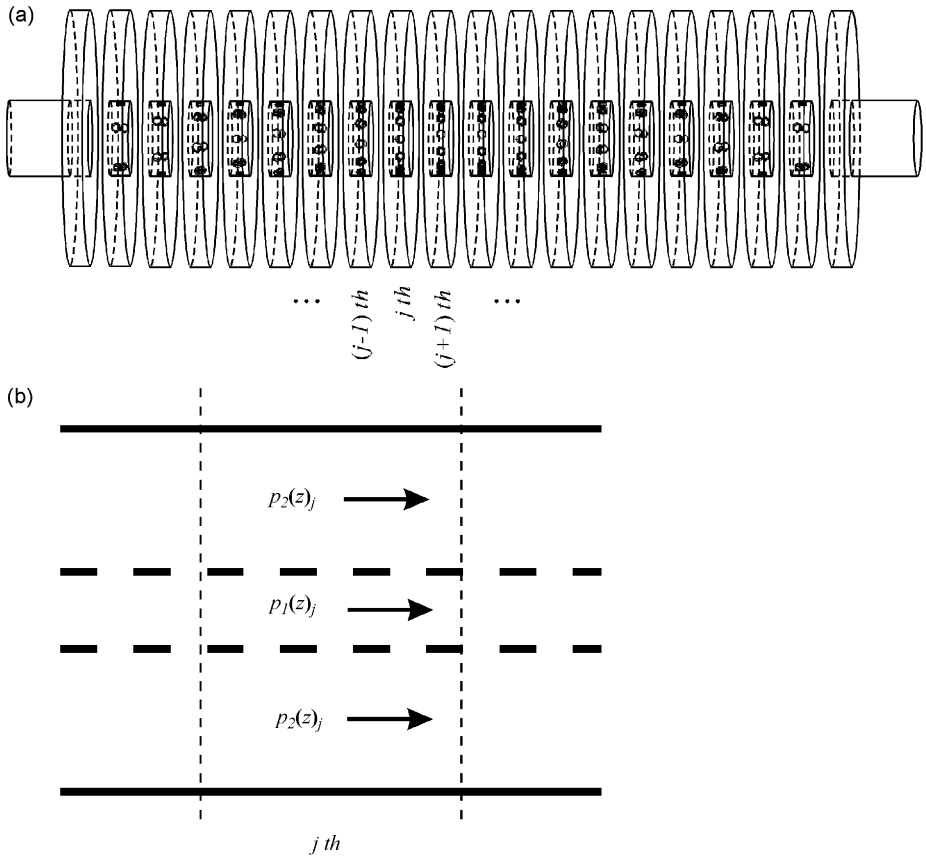

Fig. 5. Divided sections for the prediction of transmission loss in a concentric resonator using the decoupling analysis technique. (a) Overall shape and (b) simplified two-dimensional sketch for the *j*th section.

2.2. Mechanical performance

2.2.1. Flow field

The distribution pattern affects the flow field inside a resonator. Accordingly, the mechanical performance of resonators can be influenced by a change in magnitude and direction of the flow velocity along the axial distance. Changes in flow and pressure fields were investigated in a concentric resonator with varying porosity distribution patterns using a commercially available CFD code. For the viscous turbulence simulation, the k–ε model was used, in which the solution of two separate transport equations allows the turbulent velocity and length scales to be independently determined [16]. The segregated solver, in which the governing equations are solved sequentially, was used. Fig. 7 shows the geometric shape and dimensions of the model used in the CFD code. The inlet and outlet boundaries were considered under constant velocity and pressure conditions.

The two-dimensional velocity distributions in resonators with respect to both axial and radial distances are illustrated in Fig. 8. The minus sign indicates the direction of incoming flow from the outer cavity to the inner tube. Flow circulations can be observed in the rear part of cavity. Even if the cross-flow velocity inside perforated elements is different for every axial position, the magnitude of the cross-flow velocity is much smaller than the grazing-flow velocity. Average volume flow-rates of the cross-flow along the axial distance are shown in Fig. 9. The outward and inward flow-field distributions are different due to the perforated tube pattern. In the case of patterns 2 and 5, the outflow regions are wider and inflow regions narrower than in the other cases, and the outward and inward flow velocity is high. In the case of patterns 3 and 4, the outflow regions are narrower and inflow regions wider than in the other cases, and the outward and inward flow

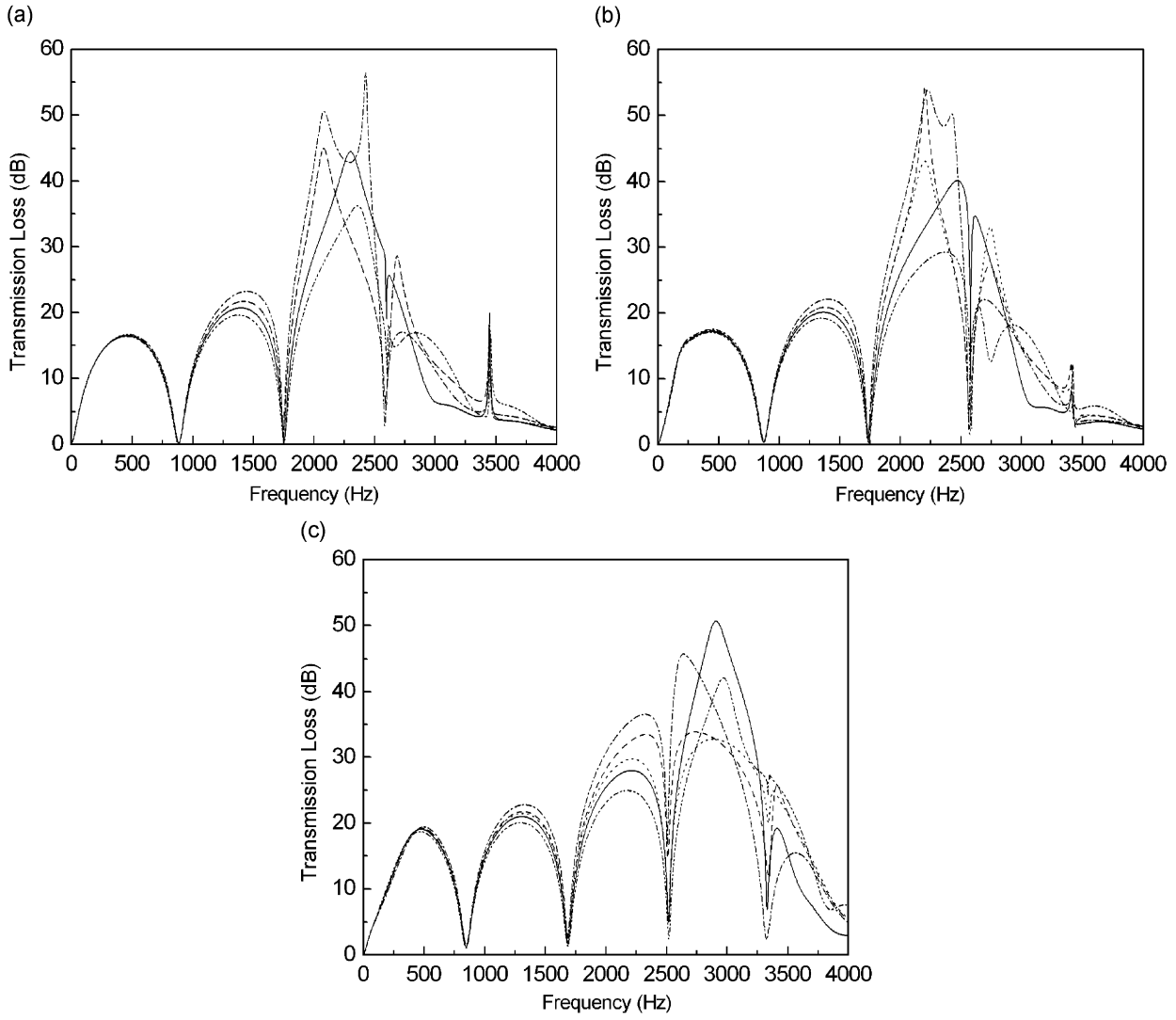

Fig. 6. Predicted transmission loss for varying distribution patterns: ——, pattern 1; — —, pattern 2; - - - -, pattern 3; — - —, pattern 4; — - - —, pattern 5. (a) $M = 0.0$; (b) $M = 0.085$; (c) $M = 0.17$.

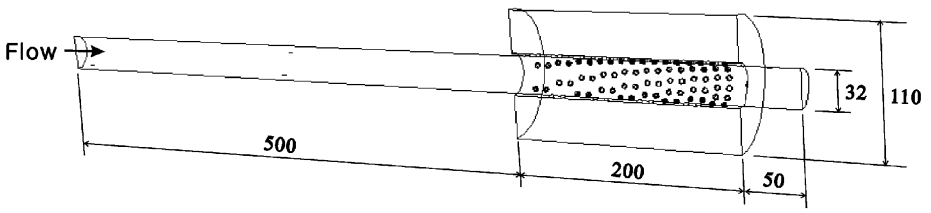

Fig. 7. Dimensions (in mm) of a concentric resonator model for CFD analysis.

velocities are low. At the inlet side of the resonator, the outward volume flow rates of patterns 1, 2, and 5 are greater than those of patterns 3 and 4. It is evident that patterns 3 and 4 show smooth flow paths from the inner tube to the outer cavity and from the outer cavity to the inner tube. However, patterns 2 and 5 show restrictions in flow field distribution. Fig. 9 illustrates the static pressure distributions. Patterns 3 and 4 show

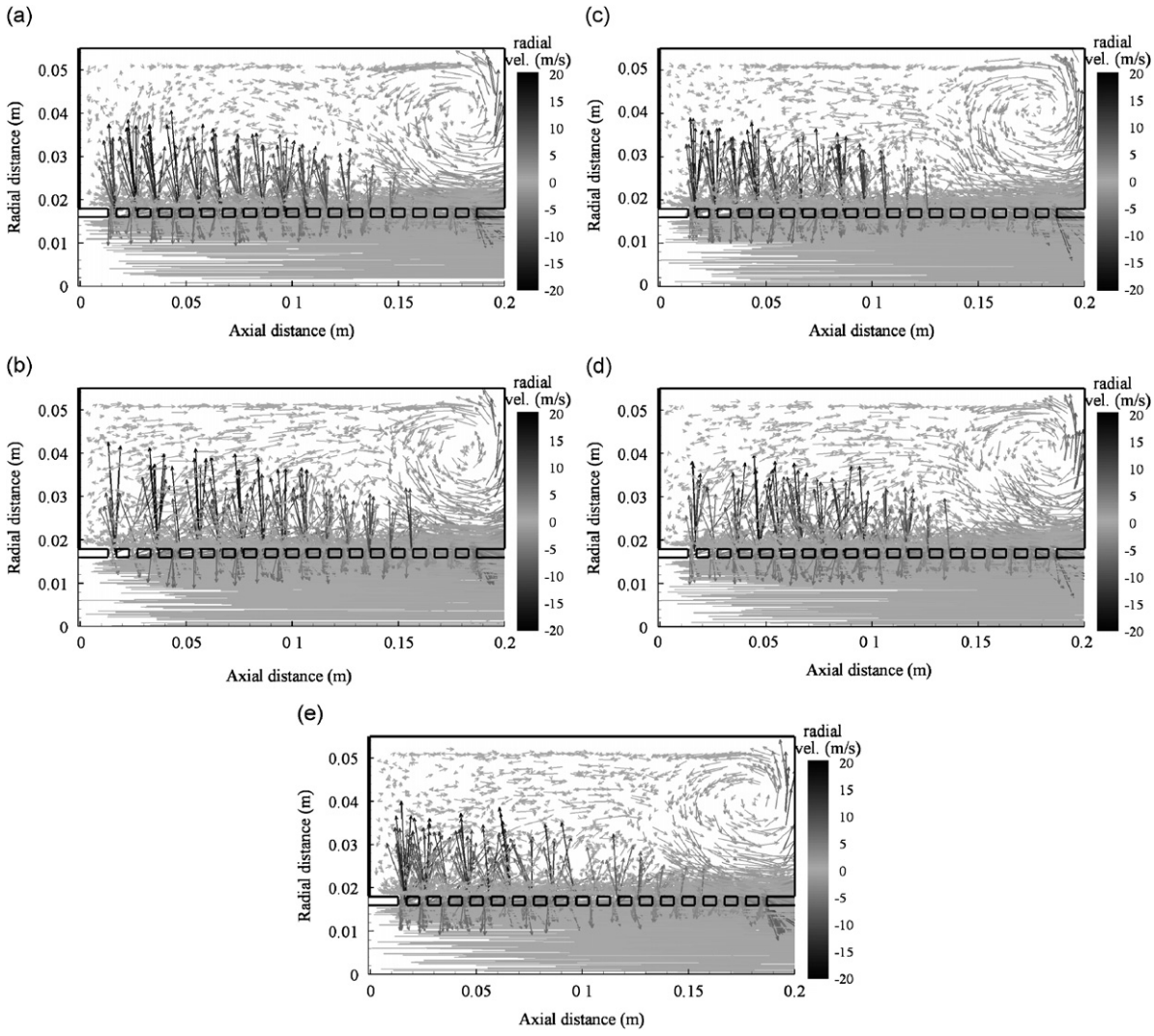

Fig. 8. Average two-dimensional flow velocity distribution for each resonator in Table 1 ($M = 0.17$; ID $\varnothing 32$ mm; OD $\varnothing 110$ mm). (a) Pattern 1; (b) pattern 2; (c) pattern 3; (d) pattern 4; (e) pattern 5.

gradually decreasing pressure distributions in the rear part of the resonator, whereas patterns 2 and 5 display an abruptly decreasing pressure pattern. The gradual decreases in patterns 3 and 4 can be explained by the ease of the flow path formation.

2.2.2. Back pressure

As a mechanical performance index, back pressure is generally defined as the stagnation pressure difference through a muffler element [17]. The stagnation pressure is defined by

$$p_o = p + \tfrac{1}{2}\rho_o V^2, \tag{3}$$

where p_o is the stagnation pressure, p the static pressure, ρ_o the density of the medium, V the mean flow velocity, and the second term on the right-hand side represents the dynamic pressure. From a practical point of view, large back pressure from an element leads to a high load on the engine and low efficiency of the mechanical performance. In this study, the static pressure difference was used as the back pressure, under the assumption that the mean flow velocity in upstream and downstream ducts is same. The back pressure was

measured using a micro-manometer (Furness Controls, FC012) connected to a pressure tap mounted on upstream and downstream ducts, as depicted in Fig. 3. The air flow was supplied by an air compressor. The mean flow velocity was measured using Pitot tube and micro-manometer. The measured static pressure difference between the pressure taps was regarded as the back pressure. Measurement was carried out under very carefully tested and controlled conditions because the static pressure was quite sensitive to the measuring environment.

The back pressure was predicted using the CFD analysis under the same simulation conditions as in Section 2.2.1. Again, the static pressure drop through the resonator was calculated as the back pressure.

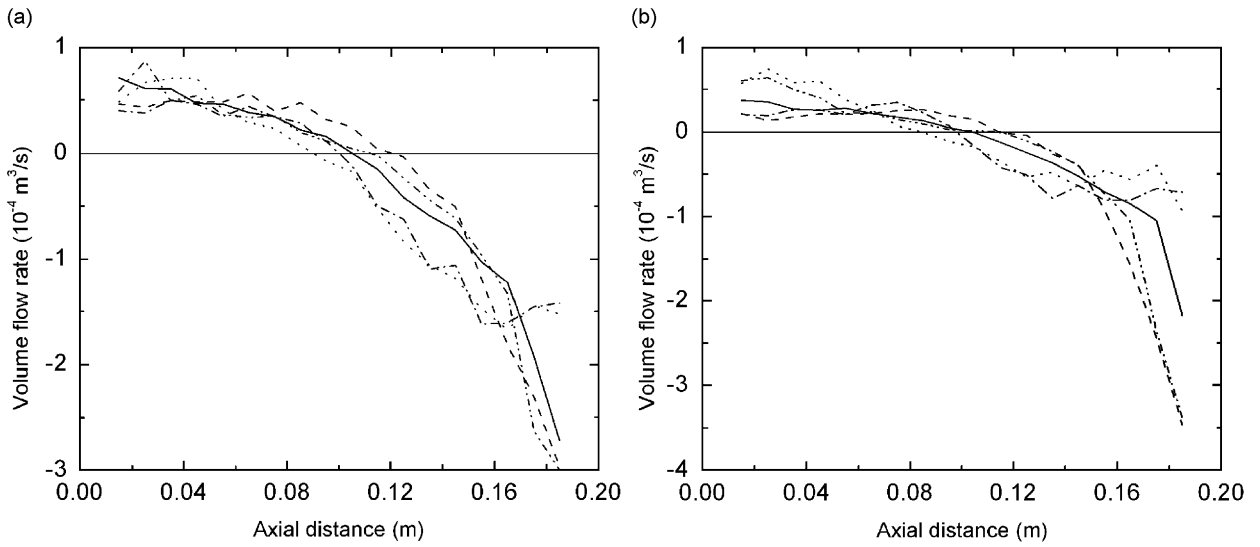

Fig. 9. Average volume flow rate of the cross-flow with respect to axial distance from the inlet position: ——, pattern 1; — —, pattern 2; - - - - -, pattern 3; — - —, pattern 4; — - - —, pattern 5. (a) $M = 0.085$; (b) $M = 0.17$.

Table 2
Measured back pressure for five perforation distribution patterns of the inner tube

Mach number	Pressure (Pa)				
	Pattern number				
	1	2	3	4	5
0.085	281.6	281.5	275.3	268.7	283.2
0.17	1074	1075	1052	1058	1122

Table 3
Predicted back pressure for five perforation distribution patterns of the inner tube

Mach number	Pressure (Pa)				
	Pattern number				
	1	2	3	4	5
0.085	250.9	254.4	251.9	250.9	257.2
0.17	870.7	876.3	862.1	864.1	880.6

Tables 2 and 3 show measured and predicted back pressure for varying distribution patterns. One can find that the predicted back pressure is less than the measured one. In the measurement, the midstream flow velocity was measured by the Pitot-tube and micro-manometer, and then the Mach number of the flow was obtained. The Mach number in a test duct was assumed to be 85% of the mid-stream velocity [17]. Errors involved in the measurement of midstream flow velocity and conversion to the Mach number can cause the discrepancies between measured and predicted back pressure. The measured and predicted back pressure showed very similar trends. The largest back pressure was obtained for pattern 5, regardless of Mach numbers. This means that pattern 5 can result in a high load on the engine and low efficiency. Patterns 1 and 2 had intermediate values. It was noted that the back pressure for patterns 3 and 4 was lowest when the flow velocity was very small ($M = 0.085$) and the same was true when the flow velocity increased two-fold ($M = 0.17$). The difference in back pressure between the largest and smallest values is approximately 3–7% of the largest back pressure, which is not negligible in terms of engine performance. From the measured and predicted performances explained in previous sections, it is evident that perforation distribution patterns 3 and 4 showed good performance from both mechanical and acoustic angles.

3. Discussion

The foregoing measurements and simulations reveal that pattern 4, in which the porosity gradually increases to a high value and then gradually decreases from the middle to the initial low porosity value, can be regarded as the most optimized perforation pattern from the point of view of the acoustic performance, i.e., TL, and mechanical performance, i.e., back pressure, of all the patterns tested. Pattern 3, in which the porosity monotonically decreases from a high value to a very low one, can be considered the next preferable one. In contrast, pattern 5, in which the porosity gradually decreases first and then gradually increases from the middle, showed the worst acoustic and mechanical performances. Pattern 2, in which the porosity monotonically increases from a very low value to a high one, is the next worst one. The performance of the uniformly perforated pattern, i.e., pattern 1, is between these two extremes. All the effects caused by the hole distribution pattern can be explained in two ways. Differences in the acoustic performance can be explained by a smooth change in wall impedance and a quarter-wavelength resonance of equivalent extended tube. Differences in the mechanical performance can be explained by a smooth change in the flow field distribution.

At the inlet and outlet of the inner tube of a resonator, which are usually connected to an unperforated, hard metal tube, the wall impedance is almost infinite. The wall impedance of a perforated element is determined by the porosity through

$$Z_{\text{wall}} = \frac{1}{\sigma} Z_{\text{orifice}}, \tag{4}$$

where Z_{wall} is the impedance of a perforated element, Z_{orifice} the impedance of one orifice, and σ is the porosity (Fig. 10). Fig. 11 shows the porosity distribution patterns and normalized wall impedance of the five different inner tubes in Table 1 and Fig. 2. Pattern 4 has the smoothest change in impedance at the two junctions of the inlet and outlet regions, which has a low-impedance region in the middle. The incident sound is gradually reflected from the perforated pipe to the source region starting with a high reflection ending in the middle part with a low reflection; reverse pattern of sound reflections exist in the later half of the perforated section. Comparing pattern 4 with pattern 5, the former starts with a high impedance value, but the amount of impedance mismatch at the entrance region is smaller than that of pattern 5. With the same average impedance in axial direction of the layers of discontinuity, a layer pattern with high impedance mismatch in the initial layer will reflect the sound energy slightly more than a layer with high impedance at the initial layer but with small impedance mismatch. Fig. 12 compares the upstream reflection coefficients of five patterns, from which one can confirm the aforementioned fact very clearly. The reflected sound from the termination, which propagates to the resonator in the reverse direction, will experience the same thing and, then, the downstream reflected wave will be small in this case. In overall, the gradual impedance matching of the perforated section cannot result in a big change in acoustic performance due to the change of perforation pattern in axial direction. This conclusion suggests that the premise of the previous work [3], viz., impedance matching at the perforated inner pipe is important for enhancing the acoustic performance, cannot properly explain the

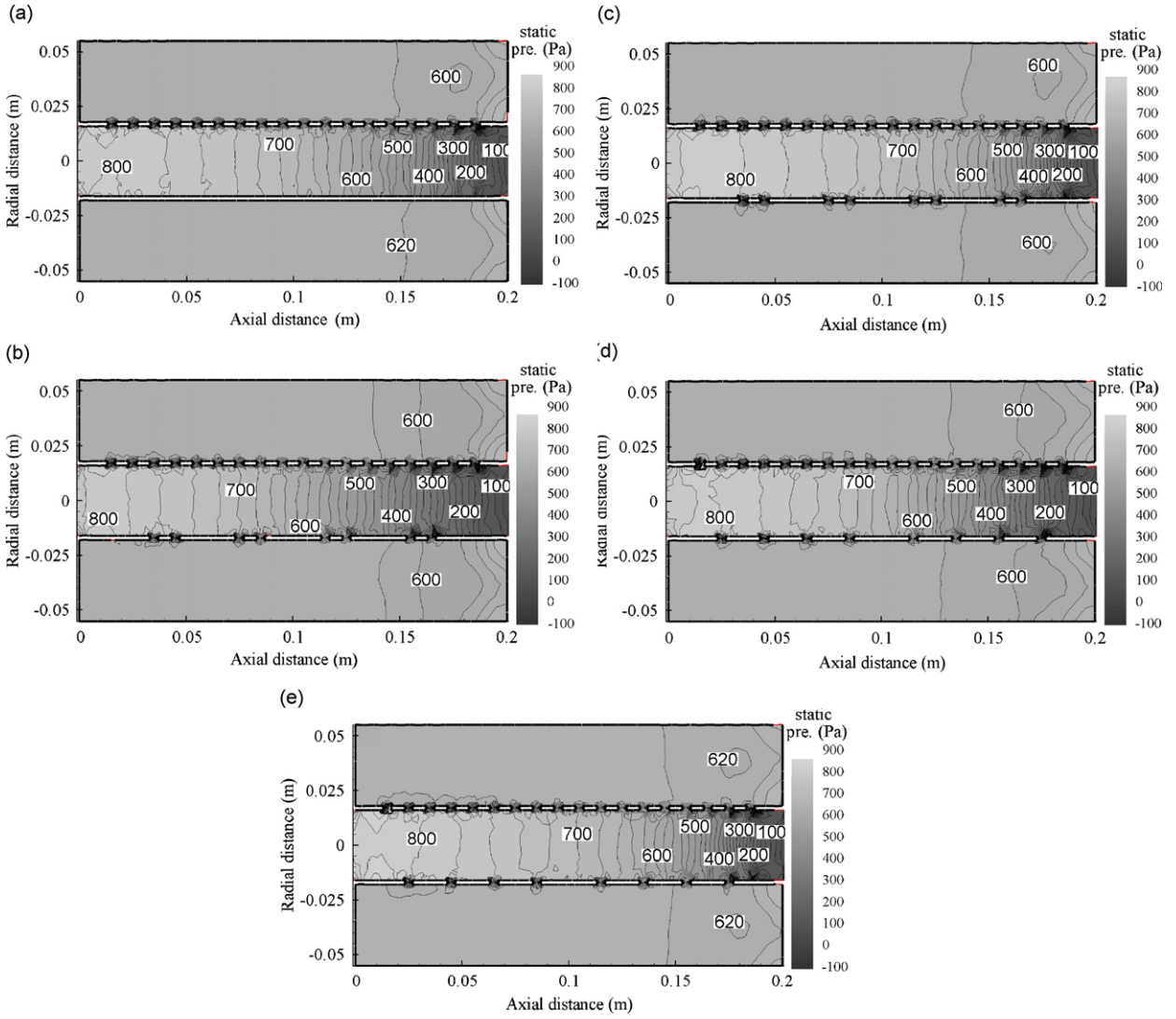

Fig. 10. Average static pressure distribution in each resonator ($M = 0.17$). (a) Pattern 1; (b) pattern 2; (c) pattern 3; (d) pattern 4; (e) pattern 5.

physics of sound attenuation in some frequency bands. However, if one observes the fact that the main difference in acoustic performance is confined to a frequency range only, a simple and physically sound explanation can be found.

As mentioned before, the TL curve for each pattern has a definite difference in its third lobe, which ranges from approximately 1.75–3 kHz. One can recall that the acoustical behavior resembles that of a simple expansion chamber with extended inlet and outlet pipes, which is affected by the quarter-wavelength tube resonance. For investigating the similarity of these two types of reactive silencer elements, the acoustic performance of uniformly perforated concentric resonator, having the average porosity, with extended inlet/outlet was calculated first. Fig. 13 shows the predicted TL curves of uniformly perforated concentric tube resonator ($\sigma = 10\%$, 25%) having extended inlet/outlet with different extension lengths and those of expansion chambers with same extended inlet/outlet tubes. Here, L_1 and L_2 mean the lengths of extended inlet and outlet, respectively. In Fig. 13, one can find that the TL peak due to quarter-wavelength resonance of extended pipes moves to low-frequency region with decreasing porosity. Therefore, one can say that the

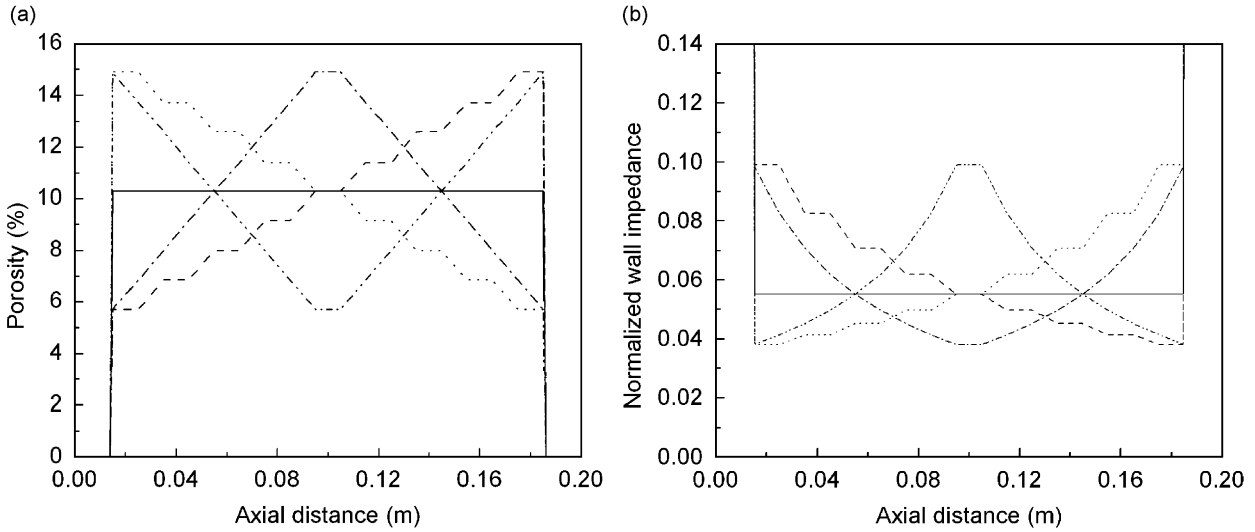

Fig. 11. Comparison of (a) porosity and (b) normalized impedance for the five perforated inner tubes in Table 1: ——, pattern 1; — —, pattern 2; - - - - -, pattern 3; — - —, pattern 4; — - - —, pattern 5.

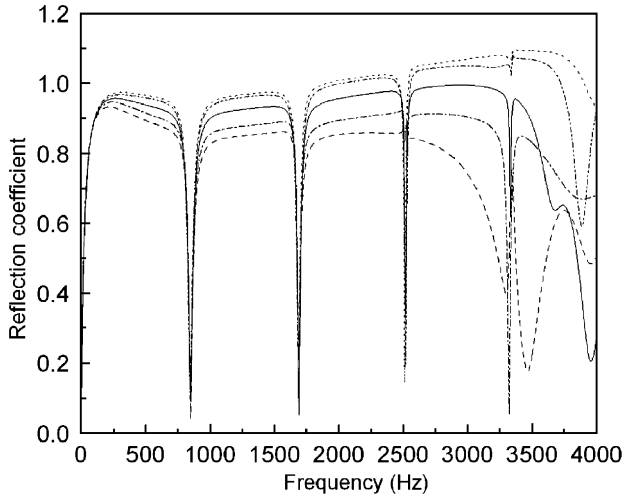

Fig. 12. Predicted upstream reflection coefficient in each distribution pattern ($M = 0.17$): ——, pattern 1; — —, pattern 2; - - - - -, pattern 3; — - —, pattern 4; — - - —, pattern 5.

perforated pipe with low porosity, located in the middle of the chamber, would construct an equivalent configuration of long extended inlet and outlet in the viewpoint of acoustic performance. From the predicted and measured TL values of five perforation patterns considered in this study, the TL peak at the third lobe moves slightly to the low-frequency region in patterns 2, 3, and 4, whereas that of pattern 1 is slightly shifted to the high-frequency region. It can be interpreted that resonators with patterns 2, 3, and 4 acts like expansion chambers having longer extended inlet/outlet length than resonators with patterns 1 and 5. From these facts, five distribution patterns in porosity can be simplified by a pattern with uniform porosity distribution having different extended inlet and outlet lengths. TL curves of concentric resonators with uniform perforation having different extended inlet/outlet lengths are shown in Fig. 14. It was assumed that the porosity of 6% or

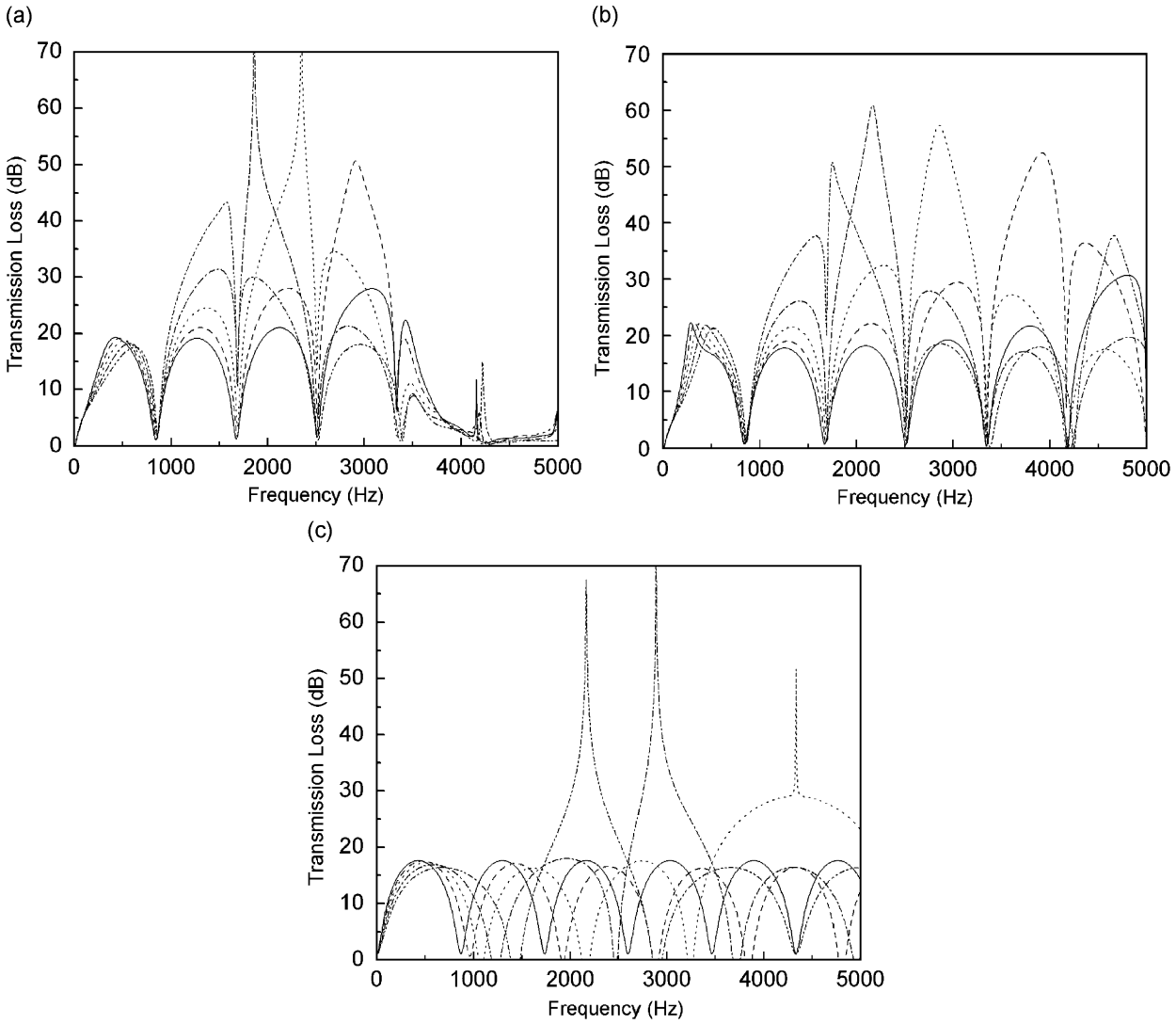

Fig. 13. Predicted transmission loss varying the extended inlet/outlet length ($M = 0.17$): ——, $L_1 = L_2 = 0$; — —, $L_1 = L_2 = 0.01$; - - - - -, $L_1 = L_2 = 0.02$; — - —, $L_1 = L_2 = 0.03$; — - —, $L_1 = L_2 = 0.04$. (a) Uniformly perforated concentric resonator ($\sigma = 10\%$), (b) uniformly perforated concentric resonator ($\sigma = 25\%$), (c) expansion chamber.

15% at inlet or outlet correspond to the extended pipes which are longer or shorter by 0.005 m, respectively, than the pipe with original length. Because it is not simple to calculate an exact equivalent length of the extended tube corresponding to a specific porosity pattern, the added length due to perforates was assumed to be equal to the half of segment length. Although the magnitudes of the third lobe of predicted TL curves in Fig. 14 are slightly different from the values in Fig. 6, the downshift of TL peak at the third lobe has a trend similar to that in the foregoing figure.

From the calculated results for flow fields in resonators, patterns 3 and 4 show a small outward volume flux in the upstream part of the inner pipe: the length of the outflux region of the inner pipe is nearly the same as that of the influx region, and the incoming volume flux is also small in the downstream part. In contrast, patterns 2 and 5 have a common feature of a large outflux in the upstream part of the resonator: the length of the outflux region of the inner pipe is greater than that of the influx region and the incoming volume flux is also large in the downstream part. Under these conditions, flow passing through the inner pipe loses an

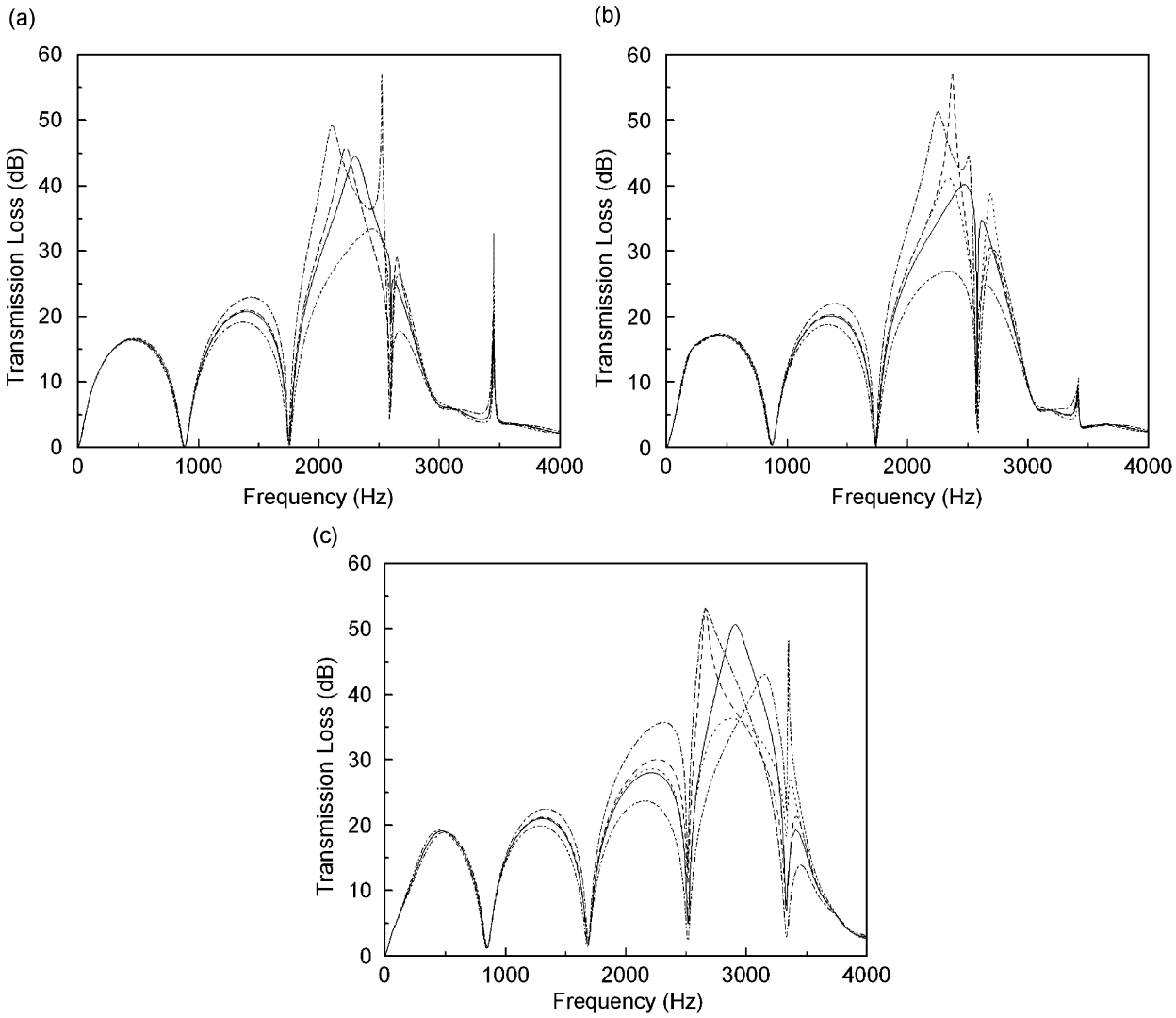

Fig. 14. Predicted transmission loss of uniformly perforated concentric resonator varying the extended inlet/outlet length: ——, $L_1 = L_2 = 0.01$; — —, $L_1 = 0.015$: $L_2 = 0.005$; - - - - -, $L_1 = 0.005$: $L_2 = 0.015$; — - —, $L_1 = L_2 = 0.015$; — · · —, $L_1 = L_2 = 0.005$. (a) $M = 0$, (b) $M = 0.085$, (c) $M = 0.17$.

appreciable amount of momentum. In other words, patterns 3 and 4 lead to smooth flow paths (or slow and small flow flux) from the inner tube to the outer cavity and vice versa. In contrast, patterns 2 and 5 have largely changing flow fields. The predicted pressure fields in the resonators also show the same trend. The static pressure of patterns 3 and 4 gradually decreased in the inner tube by a relatively small amount because of the aforementioned slow and small change in flow flux. The mechanical performance, viz., the back pressure, is highly correlated to the ease of flow through the inner tube without appreciable change in momentum.

Therefore, in designing a silencing system with concentric resonators, a distribution pattern of holes on the inner pipe should be intentionally chosen to improve the acoustic and mechanical performances under the restriction of a fixed volume. From both an acoustic and mechanical point of view, the perforated inner tube should have a smooth change in perforation pattern (or porosity), thus forming a flow field with minimized loss.

4. Conclusions

Acoustic and mechanical effects of the distribution pattern of holes in a concentric resonator were studied experimentally and theoretically. Measurements were carried out using a microphone array. The acoustic performance of the perforated resonator was calculated using sectional modeling of the inner pipe, hole, and backing cavity. The flow field in the resonator and the resultant back pressure were calculated numerically by a CFD analysis. It was observed that the most optimized perforation pattern in terms of TL and back pressure was that with gradually increasing porosity from the upstream part and gradually decreasing porosity from the middle to the downstream end. The opposite pattern for perforation distribution showed the worst acoustic and mechanical performance. The TL difference between the best and worst cases was approximately 30 dB in one situation ($M = 0.085$, third lobe); the difference between the best and uniformly perforated cases was approximately 25 dB in the same situation. For a higher flow velocity ($M = 0.17$), the former difference was about 13 dB and the latter was about 8 dB in the third lobe. The reason why the pattern with smoothly changing porosity results in a high TL value, in particular at a specific frequency range only, could be explained by an equivalent expansion chamber with extended inlet and outlet: this explanation contradicts with the previous premise stating that the acoustic performance can be enhanced by designing a smooth change in axial distribution pattern of porosity. In terms of mechanical performance, a perforation pattern with monotonically decreasing porosity from a high to a low value represents another preferable pattern as a perforated bridge. This phenomenon can be explained by considering the gradual change in wall resistance, which results in small and gradual change in flow volume and direction inside the resonator. The difference in back pressure between the best and worst cases was approximately 3–7% of the largest back pressure, which is not negligible in terms of engine performance. Consequently, for concentric resonators, it was observed that the acoustic and flow characteristics are inter-related: a gradual change in perforate impedance in the wall can improve both the mechanical and acoustic performance. It was also found that a gradual change in porosity in the downstream part of the resonator is important. In the design of silencers with a perforated resonator, careful allocation of the hole porosity on the tube would be beneficial in maximizing both the acoustic and mechanical performance, which are usually considered as having a trade-off relation, under a predetermined fixed volume of the system. Further study may lead to an optimal perforation distribution pattern having the best characteristics for both TL and back pressure.

Acknowledgments

This work was partially supported by the BK Project. The authors would like to thank Mr. Antoine Delaigue for his contribution in the initial stage of this work.

References

[1] L.L. Beranek, I.L. Vér, *Noise and Vibration Control Engineering: Principles and Applications*, Wiley, New York, 1992 (Chapter 10).
[2] D. Davis, G. Stokes, D. Moore, G. Stevens, Theoretical and experimental investigation of mufflers with comments on engine exhaust design, NACA Report 1192, 1954.
[3] F.B. Shenoda, A new silencer with good matching performance for air ducts and exhaust systems, *Acustica* 50 (1982) 338–341.
[4] Y.-H. Kim, D.-B. Yoon, An experimental study of the acoustic characteristics of perforated pipe in terms of wavenumber and porosity, *Journal of Sound and Vibration* 183 (1995) 115–127.
[5] K. Jayaraman, K. Yam, Decoupling approach to modeling perforated tube muffler components, *Journal of the Acoustical Society of America* 69 (1981) 390–396.
[6] M.L. Munjal, K.N. Rao, A.D. Sahasrabudhe, Aeroacoustic analysis of perforated muffler components, *Journal of Sound and Vibration* 114 (1987) 173–188.
[7] K.S. Peat, A numerical decoupling analysis of perforated pipe silencer elements, *Journal of Sound and Vibration* 123 (1988) 199–212.
[8] P.T. Thawani, K. Jayaraman, Modeling and applications of straight-through resonators, *Journal of the Acoustical Society of America* 73 (1983) 1387–1389.
[9] S.-H. Lee, J.-G. Ih, Empirical model of the acoustic impedance of a circular orifice in grazing mean flow, *Journal of the Acoustical Society of America* 114 (2003) 98–113.
[10] J.W. Sullivan, M.J. Crocker, Analysis of concentric tube resonators having unpartitioned cavities, *Journal of the Acoustical Society of America* 64 (1978) 207–215.

[11] J.-G. Ih, B.-H. Lee, Analysis of higher-order mode effects in the circular expansion chamber with mean flow, *Journal of the Acoustical Society of America* 77 (1985) 1377–1388.
[12] J.-G. Ih, B.-H. Lee, Implication of geometric factors of simple expansion chambers for their acoustic performance, *Proceedings of the International Noise and Vibration Control Conference (Noise '93)* 3 (1993) 155–160.
[13] J.Y. Chung, D.A. Blaser, Transfer function method of measuring in-duct acoustic properties. I. Theory, *Journal of the Acoustical Society of America* 68 (1980) 907–913.
[14] S.-H. Jang, J.-G. Ih, On the multiple microphone method for measuring in-duct acoustic properties in the presence of mean flow, *Journal of the Acoustical Society of America* 103 (1998) 1520–1526.
[15] M. Abom, H. Boden, Error analysis of two-microphone measurements in ducts with flow, *Journal of the Acoustical Society of America* 83 (1988) 2429–2438.
[16] B.E. Launder, D.B. Spalding, *Lectures in Mathematical Models of Turbulence*, Academic Press, London, UK, 1972.
[17] M.L. Munjal, *Acoustics of Ducts and Mufflers*, Wiley, New York, 1987.